CrossMark
click for updates

View Article Online
View Journal

Materials
Horizons

Accepted Manuscript

This article can be cited before page numbers have been issued, to do this please use: X. Luo, L. Liu, K. Liu, P. Gao, W. Kong, Z. Zhao, M. Pu and C. Wang, *Mater. Horiz.*, 2017, DOI: 10.1039/C6MH00535G.

This is an Accepted Manuscript, which has been through the Royal Society of Chemistry peer review process and has been accepted for publication.

Accepted Manuscripts are published online shortly after acceptance, before technical editing, formatting and proof reading. Using this free service, authors can make their results available to the community, in citable form, before we publish the edited article. We will replace this Accepted Manuscript with the edited and formatted Advance Article as soon as it is available.

You can find more information about Accepted Manuscripts in the author guidelines.

Please note that technical editing may introduce minor changes to the text and/or graphics, which may alter content. The journal's standard Terms & Conditions and the ethical guidelines, outlined in our author and reviewer resource centre, still apply. In no event shall the Royal Society of Chemistry be held responsible for any errors or omissions in this Accepted Manuscript or any consequences arising from the use of any information it contains.

ROYAL SOCIETY
OF CHEMISTRY

rsc.li/materials-horizons

View Article Online
DOI: 10.1039/C6MH00535G

Evanescent Bessel beam has attracted a lot of research interest due to its long-range sub-diffraction characteristic. In this work, we provide a novel hybrid approach to generate and record the evanescent Bessel Beam with sub-diffraction resolution about 65 nm (0.18λ) at a working distance as long as 100 nm (0.27λ). Different from any current work, our design provides the first combination of the hyperbolic metamaterial (HMM), plasmonic cavity and spin angular momentum. Excited by a concentric annular grating and filtered by HMM, a bulk plasmon polariton (BPP) modes with ultra-high spatial frequencies could be obtained. At the same time, the vectorial electrical fields could be subtly modulated by the plasmonic cavity lens. The created needle-like evanescent Bessel beam has the potential to be applied as a virtual light probe for near-field optical imaging, sensing and lithography techniques.

Published on 25 January 2017. Downloaded by Freie Universitaet Berlin on 26/01/2017 00:30:51.

Materials Horizons Accepted Manuscript

View Article Online
DOI: 10.1039/C6MH00535G

Materials Horizons

COMMUNICATION

Nanofocusing of circularly polarized Bessel-type plasmon polaritons with hyperbolic metamaterials†

Received 00th January 20xx,
Accepted 00th January 20xx

DOI: 10.1039/x0xx00000x

www.rsc.org/

Ling Liu, [#ab] Ping Gao, [#a] Kaipeng Liu, [#a] Weijie Kong,[a] Zeyu Zhao,[a] Mingbo Pu,[a] Changtao Wang,[a] and Xiangang Luo[*a]

Published on 25 January 2017. Downloaded by Freie Universitaet Berlin on 26/01/2017 00:30:51.

A miniature evanescent Bessel beam generator is realized by utilizing the combination of metasurfaces based on concentric grating and hyperbolic metamaterials composed of alternative metal/dielectric multilayer. After introducing the plasmonic cavity lens, the feature size could be compressed to 62 nm (0.17λ_0) at the wavelength of 365 nm with a working distance as large as 100 nm. The theoretical model are verified by a set of experiments, providing a promising way for the controlling of light at the nanoscale.

The Bessel beams first proposed by Durnin are typically referred to as diffraction-free beams.[1,2] Since the introduction of this concept, Bessel beams have attracted a great number of research interest, yet most works focus on the propagating Bessel beams whose dimensions are still restricted by the diffraction limit.[3-14] Evanescent Bessel beams, which could retain the transverse profile with a subwavelength size during the propagation over a near-field distance, are solutions of Maxwell's equations, too. In 1998, evanescent Bessel beams were theoretically realized through the total internal reflection of propagating Bessel beams,[15] which was later experimentally verified.[8,16] Since then, several other methods of producing evanescent Bessel beams have been proposed. In the near-field plates approach proposed by Imani and colleagues, a nonperiodically structured surface which could tailor the electromagnetic near field is designed to form a subwavelength evanescent Bessel beam.[17] In addition, the spectrum of a Bessel beam could be approximatively constructed by filtering the incident field. For example, Pendry showed that a point source located close to a thin dielectric slab could produce a cylindrical surface wave that generates an evanescent Bessel beam with central spot size of ~0.34λ_0 maintained for a distance of 0.14λ_0.[7] Subsequently, the generation of evanescent Bessel beams was validated by Zhan's group, using highly focused cylindrical vector beams and the gigantic transmission band-edge resonance in one dimensional photonic band-gap structures.[18,19] The full width at half maximum (FWHM) of the central spot is larger than 0.3λ_0 (~190 nm).[18] Zhan *et al*. also proposed and experimentally verified that evanescent Bessel beam could be generated by angularly filtering the radially polarized light using surface plasmon (SP) resonance.[20,21] A spot as small as 195 nm with 532 nm optical excitation is obtained.[21] Restricted by the refractive index of material and approach of launching high spatial frequency modes, the FWHM could not be further reduced at the working wavelength. Despite the fact that catenary nanoapertures could generate both propagating and evanescent Bessel beams,[6,10] the polarization conversion effeciency is often limited.

Fortunately, the bulk plasmon polaritons (BPPs) generated by hyperbolic metamaterial (HMM) provides a fascinating candidate to get high spatial frequency modes. The BPP modes, namely super-plasmonic modes, are generated through the mutual coupling of plasmonic polaritons between adjacent metal-dielectric layers.[22-24] Compared with normal SP modes, the BPP modes with higher spatial frequency could provide a focus with smaller size beyond the diffraction limit.

In this paper, an evanescent Bessel beam with sub-diffraction characteristic is generated by utilizing HMM composed of alternative metal and dielectric layers, along with the concentric metasurface and plasmonic cavity lens in the form of Ag-Photoresist-Ag structure.[25] This method is based on the launch of high spatial frequency BPP modes, the spatial frequency filtering characteristic of HMM as well as the vectorial fields modulation ability provided by the plasmonic cavity lens. Numerical simulations indicate that an evanescent Bessel beam with a central spot size of 62 nm (0.17λ_0) could be maintained for a distance as large as 100 nm, and the experiment results also verify that the focusing spot could be compressed to about 65 nm beyond the diffraction limit. It is

a. State Key Laboratory of Optical Technologies on Nano-Fabrication and Micro-Engineering, Institute of Optics and Electronics, Chinese Academy of Science, P.O. Box 350, Chengdu 610209, China.
b. University of Chinese Academy of Sciences, Beijing 100049, China.
* Correspondence and requests for materials should be addressed to X.G.L. (e-mail: lxg@ioe.ac.cn)
#These authors contributed equally to this work.
† Electronic Supplementary Information (ESI) available. See DOI: 10.1039/x0xx00000x

Materials Horizons Accepted Manuscript

View Article Online
DOI: 10.1039/C6MH00556G

Published on 25 January 2017. Downloaded by Freie Universitaet Berlin on 26/01/2017 00:30:51.

believed that this method has potential applications in nanolithography, super-resolution imaging and high density optical storage, etc.

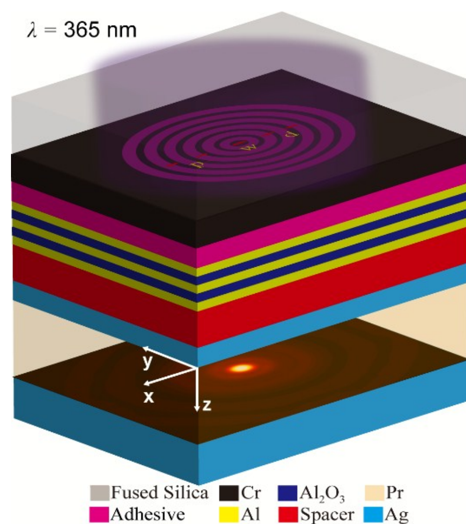

Fig.1 Schematic of the Al/Al_2O_3 hyperbolic metamaterial and Ag/Pr/Ag plasmonic cavity lens for the evanescent Bessel beam generation under circular polarization illumination.

Figure 1 is a schematic configuration to obtain deep subwavelength evanescent Bessel beam by two structures. One is the Bessel beam generating structure composed of the HMM and the concentric annular grating, which behaves as a metasurface to couple the propagating light with evanescent wave. The other is the photoresist (Pr) recording structure in the form of a plasmonic cavity lens. The above mentioned structures are separated by a spacer layer, the thickness of which could be set as the diffraction-free distance of the evanescent Bessel beam in experiments. Circularly polarized plane wave with a wavelength of 365 nm impinges on the 40-nm-thick Cr grating from the quartz substrate. The concentric annular grating serves as a generator of high spatial frequency evanescent waves, which excites multiple orders of evanescent waves with radial wavevector k_r of $nk_0\sin(\theta_i)+m2\pi/p$ in all azimuthal directions, where k_0 and θ_i are the incident wavevector in vacuum and incident angle, respectively; n is the refractive index of substrate; p is the period of grating and m is an integral diffraction order. In the case of normal illumination, k_r is reduced as $m2\pi/p$, and it means that the diffraction wavevector only depends on the diffraction order and the period of grating. Thus, six-ring annular patterns with the innermost ring diameter of w=100 nm, the slit width of d=61 nm, and the period of p=122 nm would generate diffraction waves with the radial wavevector of $k_r=3mk_0$. The Cr grating is planarized by the adhesive with a thickness of 30 nm. Adjacent to the planarization layer is the HMM, which is composed of two layers of Al_2O_3 films centrally embedded in three Al films (15nm thickness for each layer). The Pr recording structure is composed of 20 nm thick Ag, 30 nm thick Pr, and 70 nm thick Ag. The permittivities for fused silica, Cr, Al, and Al_2O_3 at λ=365 nm are ε_{quartz}=2.13, ε_{Cr}=-8.9+9.0i, ε_{Al}=-19.46+3.6i, ε_{Al2O3}=3.218, ε_{Ag}=-2.4+0.24i, and ε_{Pr}=2.59, respectively.[26] The real part permittivity of the adhesive material measured by ellipsometer (SE 850, SENTECH) is 2.33 at 365 nm working wavelength. The other optical properties of the adhesive material are also discussed in ESI† (Fig. S1). The values of the diameter of the innermost ring and the thickness of metal and dielectric film are determined by optimization. (See ESI†. Fig. S2). The reason for choosing the metal material and how to decide the periods of the metal-Al_2O_3 are analysed in ESI† (Fig. S3), too.

Bessel beam is described by the superposition of a set of plane waves with the wavevectors lying on the surface of cone in the Fourier space.[7,18] The diffraction-free characteristic of Bessel beam emanates from the intensity distribution in the plane normal to z axis proportional to $J_0^2(k_r r)$, where J_0 is the zero-order Bessel function of the first kind, k_r is the radial wavevector and $k_r=\sqrt{k_0^2-k_z^2}$. Accordingly, the FWHM of Bessel beam is only decided by the spatial wavevector k_r.

Compared with SP modes, the BPP modes generated by HMM could provide higher spatial frequency. The HMM based on the Al/Al_2O_3 multilayer structure acts like a homogeneous electromagnetic medium with a highly anisotropic, hyperbolic spatial frequency dispersion.[27,28] Figure 2(a) is the dispersion relation of the multilayer structure, which represents the relationship between tangential wavevector k_x and longitudinal wavevector k_z.[27] The plot (black curve) of the real part of k_z for variant k_x exhibits a hyperbolic profile with no cut-off spatial frequency and evanescent waves with infinitely large wavevector could be launched by HMM when ignoring the light absorption. However, due to the quick growth of the imaginary part of k_z, the ultra-high spatial frequencies could not be supported, which makes the fact that the light modes with a specified k_x range of spatial frequencies would go through the metamaterial. Also, Fig. 2(a) clearly shows that a filtering window with low absorption for the specific BPP waves around the wavevector $3k_0$ is created through the multilayer metamaterial, resulting that the BPP wave with the wavevector $3k_0$ could be coupled out the metamaterial and other diffraction waves outside the window range are damped. As expected, the calculated two-dimensional optical transmission function (OTF) for the proposed multilayer structure exhibits a filtering window around the wavevector $3k_0$ as shown in Fig. 2(b). The high transmission efficiency is mainly caused by the interaction of modes on the surface and the metamaterial medium.[28]

Higher radial wavevector promises a narrower FWHM of Bessel beam.[7] Thus further analysis is performed to tune the filtering window of multilayer structure towards higher spatial frequency. For the multilayer structure, the magnitude of electric field intensity in the dielectric layer is much higher than that in the metal layer. When the resonance effect of BPP wave occurs, the electric fields mainly concentrates in the dielectric layer, which is shown in Fig. 2(c). This phenomenon has been testified by the mode analyses in the MIM structure, which presents the high confining capability of waveguide mode for electromagnetic energy.[29] The multilayer could be regarded as stacks of MIM structure, thus, tuning the dielectric layer is anticipated to change the position of filtering window. The simulation is rendered by calculating the OTF distribution of multilayer versus the permittivity (Fig. 2(d)) and thickness (Fig. 2(e)) of dielectric layer, which shows that increasing the

Materials Horizons Accepted Manuscript

This journal is © The Royal Society of Chemistry 20xx

View Article Online
DOI: 10.1039/C6MH00535G

permittivity or decreasing the thickness could push the centre wavevector of filtering window towards higher spatial frequency.[30,31] The polarization of incidence light plays another crucial role in the generation of deep subwavelength evanescent Bessel beam, which could be clarified by analytically calculating the field distributions after the HMM with the method developed in Ref. 32. If the illumination is circularly polarized, the components in Cartesian coordinate system are expressed as:

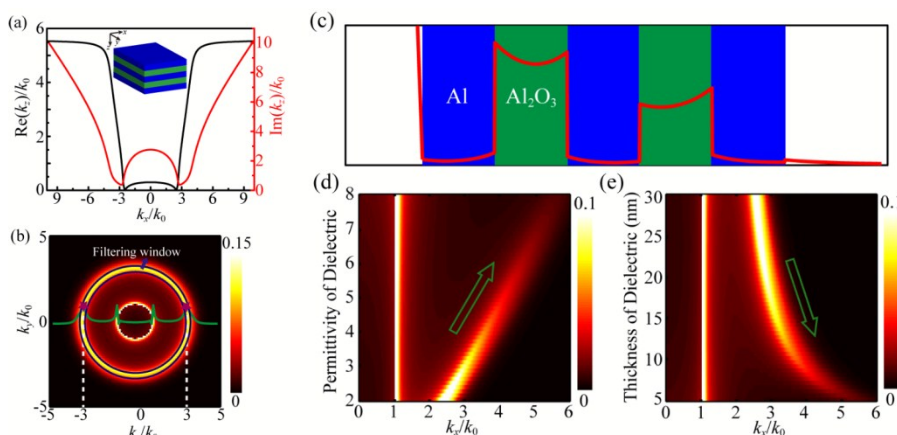

Fig.2 (a) Calculated real (black curve) and imaginary (red curve) part of longitudinal wavevector k_z for variant tangential wavevector k_x in the proposed Al/Al_2O_3 metamaterial (Inset in (a)) at the incidence light wavelength of 365 nm. (b) Two-dimensional optical transmission function (OTF) versus the tangential wavevector k_x and k_y of HMM. The olive curve in (b) is the OTF distribution along the position of k_y =0. The stars in (b) correspond to the centre position of specific BPPs coupling window in multilayer metamaterial. (c) Electric field intensity distribution (red curve) inside multilayer structure at the incident wavevector of $3k_0$. (d)(e) Calculated OTF distributions versus (d) permittivity and (e) thickness of dielectric layer in the multilayer structure. When tuning the permittivity and thickness, other parameters are kept unchanged.

$$\begin{aligned} E_x(r,\varphi,z) &= -\frac{1}{2}i\left|t(k_r)\right|k_z\exp(i\varphi)\left[\exp(i\varphi)J_2(k_r r)-\exp(-i\varphi)J_0(k_r r)\right]\exp(ik_z z) \\ E_y(r,\varphi,z) &= -\frac{1}{2}\left|t(k_r)\right|k_z\exp(i\varphi)\left[\exp(i\varphi)J_2(k_r r)+\exp(-i\varphi)J_0(k_r r)\right]\exp(ik_z z) \\ E_z(r,\varphi,z) &= -\left|t(k_r)\right|k_r\exp(i\varphi)J_1(k_r r)\exp(ik_z z) \end{aligned} \quad (1)$$

where r, φ and z are cylindrical coordinates, k_r and k_z is the radial and longitudinal wavevector with $k_r^2+k_z^2=k_0^2$, J_m is the mth-order Bessel function of the first kind and $t(k_r)$ is the transmission coefficient of diffraction wave.

According to the Eq. 1, Fig. 3(a) illustrates the relationship between the resolution of evanescent Bessel beam and the radial wavevector k_r under circular polarization illumination. As expected, the FWHM of beam could be significantly reduced by increasing the radial wavevector. At the same time, the vectorial electric field components have different contributions to the evanescent Bessel beam. The radial component intensity $|E_r|^2$, defined as $|E_r|^2=|E_x|^2+|E_y|^2$, presents a spot satisfying the zero-order Bessel function, while the longitudinal component intensity $|E_z|^2$ gives negative contribution with a doughnut distribution, as shown in the inset of Fig.3(b). For the radial component E_r, these two BPP waves would interfere constructively at the centre because all BPP waves emerging from the grating arrive at the centre with the same amplitudes and phases. However, the focusing of longitudinal components E_z would lead to the destructive interference and a null at the optical axis. Since the magnitude $|E_z|^2$ is comparable to $|E_r|^2$, the overall spot is greatly extended. Thus, we can conclude that the magnitude ratio of the electric field components determines the transverse profile of the beam after the HMM and would influence the resolution of the evanescent Bessel beam.

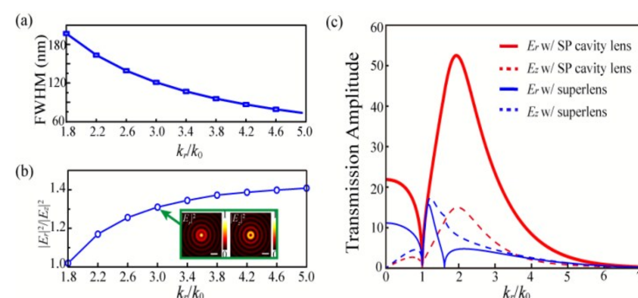

Fig.3 (a) FWHM of the intensity profile of evanescent Bessel beam through the Bessel-BPPs focusing structure and (b) Ratio of electric intensity components as a function of the radial wavevector k_r under circularly polarized illumination. The insets in (b) are the distribution of $|E_r|^2$ and $|E_z|^2$ with $k_r=3k_0$. The wavelength of incidence light is 365 nm. The geometrical parameters are the same as Fig. 1. The scale bar in insets are 100 nm. (c) Transmission amplitude of electric field components for the transverse wave vector through the structure of Ag-Pr-Ag (w/surface plasmonic cavity lens) and Ag-Pr (w/ superlens) in the Pr region.

Published on 25 January 2017. Downloaded by Freie Universitaet Berlin on 26/01/2017 00:30:51.
Materials Horizons Accepted Manuscript

View Article Online
DOI: 10.1039/C6MH00535G

Materials Horizons

COMMUNICATION

Published on 25 January 2017. Downloaded by Freie Universitaet Berlin on 26/01/2017 00:30:51.

Materials Horizons Accepted Manuscript

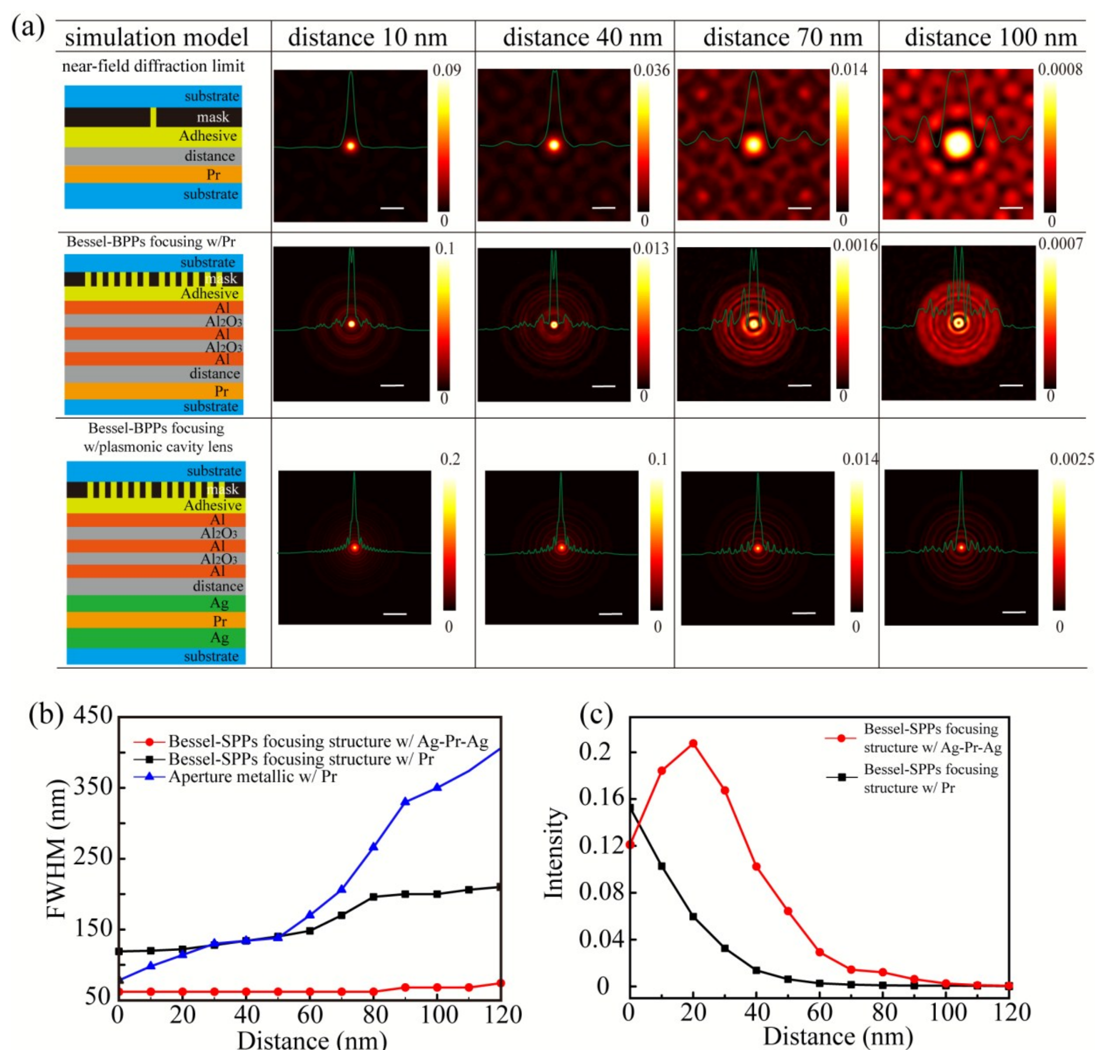

Fig. 4 (a) Cross-section of electric field intensity distributions on the plane, 15 nm away from the Pr surface for different distance. The configurations correspond to the near-field diffraction limit for a metallic slab with a 60nm diameter hole; Bessel-BPPs focusing structure with Pr recording layer and Bessel-BPPs focusing structure with plasmonic cavity recording structure, respectively. The scale bar is 300nm. (b) FWHM of the transmitted beams for different configurations versus different distances. (c) Total field intensity $|E|^2$ as a function of the distance along the *z* axis.

Fortunately, the transmission amplitudes of E_r and E_z could be effectively modulated in a broad spatial spectra by the Ag cladding, as shown in Fig.3(c). When an Ag cladding is introduced, the reflection effect of Ag cladding would modulate the electric field components and make the electric field component E_r to be dominant in the Pr region. As a result, the transmission amplitude of electric field component E_r is about 3.6 times than that of electric field component E_z at the radial wavevector of $k_r=3k_0$. Figure 3(c) also shows that with the traditional superlens structure, single Ag reflecting layer deposited on a Pr layer, the difference between the electric amplitude of E_r and E_z is not obvious at the radial wavevector of $k_r=3k_0$. Meanwhile, the dimensions of the plasmonic cavity lens composed of Ag-Pr-Ag are crucial to their optical properties, which are discussed in ESI† (Fig. S4).

Figure 4(a) is a detailed comparison of the beam propagating properties for three different configurations. The top panel of Fig. 4(a) is the near-field diffraction limit case for the metallic slab (Cr film) with 60 nm diameter hole, which shows that the FWHM of a normal light beam quickly increases after leaving the metallic slab. Maybe, the stray light field around the main spot is caused by periodic boundary

View Article Online
DOI: 10.1039/C6MH00535G

Published on 25 January 2017. Downloaded by Freie Universitaet Berlin on 26/01/2017 00:30:51.

Materials Horizons Accepted Manuscript

conditions in both the *x* and *y* directions used in simulation. The simulated results of Bessel-BPPs focusing structure without cavity lens in the middle panel of Fig. 4(a) exhibit that the hollow exists in the main lobe of the transverse profiles, confirming that the longitudinal component $|E_z|^2$ gives more negative contribution as the distance in the z direction becomes larger. At the same time, the intensity of side lobe increases as larger distance due to the interference of other diffraction waves outside the filtering window (k_r=3k_0), especially the interference of the propagation wave components. When the plasmonic cavity lens is introduced, the hollow around the focus disappears, the side lobe is further suppressed and the transverse profile of beam is remarkably compressed to about 62 nm owing to the modulation effect of electric filed components and the ability to transfer the evanescent waves in a wider wavevector range compared with the Bessel-BPPs focusing structure with Pr medium in ESI† (Fig. S5). This is mainly attributed to the reflection enhancement of evanescent waves transmitted through the top Ag layer, which is benefit from the surface plasmon excitations at the interface of Pr and bottom Ag layer. Figure 4(b) shows the FWHM of the transverse profiles for different propagating distances along the z axis for the above three excitation structures. In the Bessel-BPPs focusing structure without cavity lens, the transverse intensity profile of beam after the HMM remains unchanged over a small distance in near field region (distance from 0 nm to 20 nm), indicating the diffraction-free property of evanescent Bessel beam. However, the FWHM of diffraction-free beam is about 120 nm, which is consistent with the theoretical results from Eq. 1 as exhibited in Fig. 3(a). For Bessel-BPPs focusing structure incorporating the plasmonic cavity lens, the FWHM of the central spot of evanescent Bessel beam holds 62 nm in the distance of 0~100 nm. In the control case of a transparent hole with diameter 60 nm in the Cr film, the FWHM of the transverse profiles after the film rapidly increases and reaches to 350 nm at the distance of 100 nm, which is expanded about 5.7-folds than the case with plasmonic cavity lens. This result testifies the remarkable advantage of evanescent Bessel beam as a virtual tip in near-field probing over the near-field scanning microscopes (SNOMs). Additionally, Fig. 4(c) shows the exponential-liked trend of the electric field intensity over the distance. Although the HMM would lead to high absorption, the plasmonic cavity lens presents higher intensity due to the cavity resonance effect.

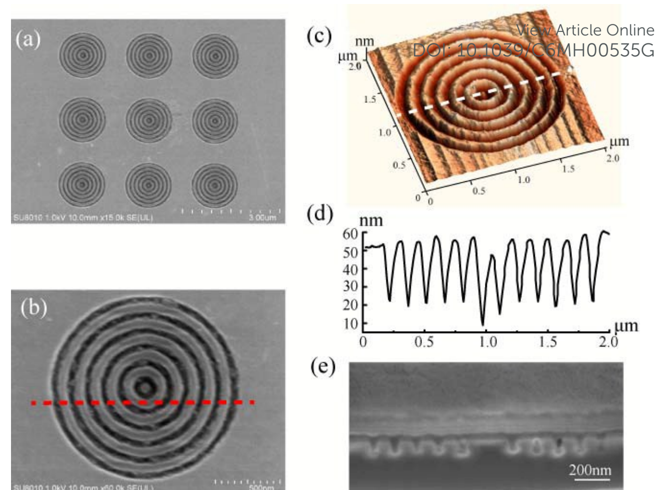

Fig.5 (a) SEM picture of the concentric annular grating array milled onto the Cr layer by FIB; (b) Magnified picture of concentric annular grating pattern in (a); (c) AFM image for the Cr concentric annular grating mask; (d) Cross sectional profile of (c) at the depicted position. (e) Cross section picture of Bessel-BPPs focusing structure along the red dashed line in (b).

Figure 5 exhibits the fabricated sample characterized by scanning electron microscope (SEM). The 3×3 array concentric annular gratings are patterned on the Cr layer in order to testify the ability of parallel fabrication. In addition, the magnified single grating pattern is shown in Fig. 5(b). Moreover, a 3D AFM image demonstrated in Fig. 5(c) further depicts the grating profile. Meanwhile, the cross sectional contour plotted in Fig. 5(d) shows the grating pattern with a pitch of 130 nm, and the average height of the gratings has been measured to ~40 nm, which is close to the expectable thickness in design. The cross section of Bessel-BPPs focusing structure is milled by FIB, and the 40 nm thick Cr film was completely etched as shown in the Fig. 5(e). Besides, the 5 stack layers of Al/Al_2O_3 are clearly shown, and the bright and grey layers are Al and Al_2O_3, respectively. The dark layer between the grating pattern and the multilayer structure is the planarization layer.

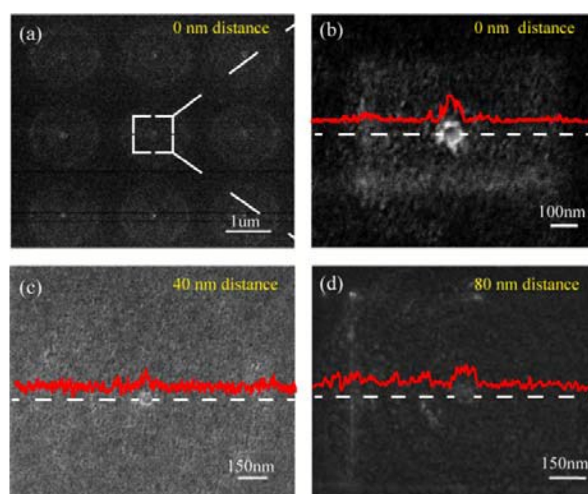

Fig.6 (a) The lithography result by Bessel-BPPs focusing structure combined with plasmonic cavity lens at the distance of 0 nm. (b) The magnified SEM picture in (a). (c) and (d) Lithography results by Bessel-BPPs focusing structure combined with plasmonic cavity lens at the distance of 40 nm and 80 nm, respectively. The red curves in (b), (c) and (d) represent the corresponding SEM image gray values along the white dashed lines.

Please do not adjust margins

View Article Online
DOI: 10.1039/C6MH00575G

Published on 25 January 2017. Downloaded by Freie Universitaet Berlin on 26/01/2017 00:30:51.

The recording patterns of Pr layer with the optimum exposure dose at different working distances in lithography processing are shown in Fig. 6. Furthermore, as an example, the effect of exposure dose on the focusing spot sizes in the lithography experiment with the fixed distance of 40 nm is explored in ESI† (Fig. S6). The experimental results with the working distance of 0 nm, shown in Fig. 6(b), exhibits the spot size of 67 nm on the Pr layer. When the distance is elongated to 40 nm, the size of spot recorded on Pr layer reaches 65 nm, as depicted in Fig. 6(c). Figure 6(d) indicates that even the distance arises to 80 nm, the spot could maintain the size of about 70 nm. Within the processing tolerant error, the experiment results also exhibit the diffraction-free characteristic of the evanescent Bessel beam in near field. The sizes of spot achieved in the experiments are inconsistent with the simulated results due to the inaccurate deposited thicknesses of the space layer and measurements. As shown in Fig. 5, the side lobes are also recorded in Pr layer at different distances, but the intensity of the side lobes are lower than that of main lobes, this means the focusing spots could be easily observed in Pr layer. Besides, the uniform flux of circular polarization illuminating light is 7 mw/cm^2, but the scattering caused by rough surface and interface of the multilayers would affect the experimental transmission coefficient, which is smaller than predicted by simulation. The SEM images of Pr recording spots are taken at the back side of illumination substrate, which convinces that the Pr exposure depth reaches 30 nm.

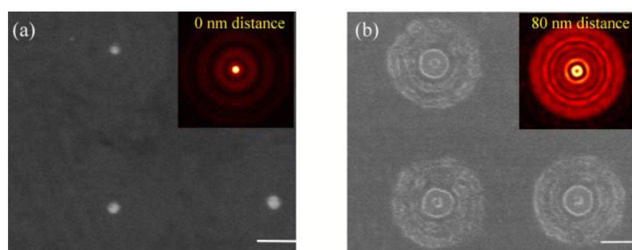

Fig.7 Simulated and experimental imaging results of Bessel-BPPs focusing structure with Pr medium. (a) The SEM image of resist patterns for the fixed distance of 0 nm. (b) The SEM image of resist patterns at 80 nm distance. The insets in (a) and (b) are the corresponding simulated images. The scale bars are both 400nm.

In addition, the experiment results of the control case of Bessel-BPPs focusing structure without plasmonic cavity lens are also obtained. As shown in Fig. 7(a), the focusing spot is only ~130nm with the distance of 0 nm, and the size of the focusing spot is approximately coordinate to the predicted results from Eq. 1 shown in Fig. 3(a), despite of the experimental errors in the fabrication processing. In the case of large distance, the doughnut patterns have been obtained in lithography experiment, which is mainly attributed to the dominant longitudinal electric field component E_z The slight inconsistency between recorded patterns shown in Fig. 7(b) and the simulated results shown in the inset of Fig. 7(b) is owing to excessive exposure dose.

Experimental methods

Fabrication of the Bessel-BPPs focusing structure incorporating plasmonic cavity lens

The fabrication flow of the Bessel-BPPs focusing structure incorporating a plasmonic cavity lens is depicted in ESI† Fig. S7(a). The Cr film with 40 nm thickness is deposited on the fused silica substrate by Magnetron Sputtering (RF power of 400W, deposition rate of 0.5nm/s and temperature of 300°C). The concentric annular grating patterns are milled onto the Cr layer by focused ion beam (Helios Nanolab 650, FEI Company, @30 kV Accelerating Voltage). The adhesive is spun to planarize the grating patterns and is cured by i-line mercury lamp with 365 nm central wavelength and energy density of 35 mJ/cm^2. The adhesive layer is RIE etched with O_2 and CHF_3 to get a planar profile with remained thickness of about 30 nm. Then two pairs Al/Al_2O_3 and Al films are deposited alternatively and sequentially on the adhesive layer by magnetron sputtering. The optimized sputtering conditions include a power of 200W in RF mode, an Ar gas flow rate of 6.8 sccm, and a base pressure of 5.0×10^{-5}Pa. The deposition rate for Al and Al_2O_3 are 0.3 nm/s and 0.06 nm/s, respectively. After that, the deposition of Al_2O_3 layer was applied as the spacer. The thickness could be set equally to the different diffraction-free distance of the evanescent Bessel beam in experiments. For the plasmonic cavity lens structure, the 20-nm-thick Ag film was first deposited onto Bessel-BPPs focusing configuration via thermal evaporation at a base pressure of 5.0×10^{-4} Pa with a deposition rate of 1nm/s. An approximately 30-nm-thick photoresist of diluted AR-P3170 (diluted by ALLRESIST GMBH, Strausberg, 30nm @ 4000rpm) was spun onto the substrate to record the near-field images. After prebaking the photoresist on a hotplate at 100 °C for 5 min, a 50-nm-thick Ag film was evaporated on the photoresist (base pressure of 5.0×10^{-4} Pa, deposition rate of 5 nm/s).

In the lithography process shown in ESI† Fig. S7(b), a LED light with 365 nm wavelength is converted to the circular polarization by a polarizer and quarter wave plate and impinges normally on the sample from the fused silica substrate side. The effect of divergent angle of the incident light on focusing spot is discussed in ESI† Fig. S8. After exposure, the 50 nm reflective Ag layer is removed physically by 3M tape. Then the Pr is developed for 40s in a mixed solution of AR 300–35 and de-ionized water with a volume ratio of 1:1 at 0℃ temperature, then rinsed by deionized water and dried by N_2.

Numerical characterisation

Numerical simulations in the Fig. 2(a) are calculated by the characteristic matrix method; Results in Fig. 2(c)-(e) and Fig. 3 are obtained using the rigorous coupled wave analysis (RCWA).[33,34] The electric field intensity distributions shown in Fig. 4 is simulated using the commercially available CST software with periodic boundary conditions in both the *x* and *y* directions, and perfectly matched layer in the *z* direction.

Conclusions

In summary, this paper presents a conceptually new approach to achieve deep subwavelength evanescent Bessel beam based

Materials Horizons Accepted Manuscript

This journal is © The Royal Society of Chemistry 20xx

Please do not adjust margins

on the launch of high spatial frequency BPP modes. Firstly, simulations demonstrate that the FWHM of the generated evanescent Bessel beam after HMM retains ~120 nm over a near-field distance of 20 nm with circularly polarized UV light illumination. Further, after employing the plasmonic cavity lens, the experiment results prove that the focusing spot with ~65 nm could be achieved at the distance of 0 nm, 40 nm and 80 nm, respectively. We believe that this is an excellent candidate for virtual probe which alleviates the proximity requirement of other near-field probing approaches. Moreover, the scheme enables us to produce higher resolution evanescent Bessel beam by increasing permittivity and decreasing thickness of dielectric layer in multilayer structure,[35-39] which exhibits great potential in biomedical imaging and the fabrication of various nanostructures.[40-44]

Author contributions

The manuscript was written through contributions of all authors. L.L., P.G. and K.L. contributed equally to this work. L.L. and K.L. performed the lithography experiments and characterized the samples. P.G. fabricated the mask patterns and milled the sample. L.L. performed numerical modeling. W.K., Z.Z. and M.P. contributed the valuable discussion for this study. C.W. suggested the use of circular polarization. L.L. and X.L. wrote the paper. X.L. conceived the original idea and supervised the project.

Acknowledgements

We acknowledge the financial support by 973 Program of China under contract No. 2013CBA01700 and National Natural Science Funds under contact Nos. 61138002 and 61575202. L.L. would like to thank W.Z. for the help in numerical simulations.

Notes and references

1 J. Durnin, *Journal of the Optical Society of America A,* 1987, **4**, 651–654.
2 J. Durnin, J. J. Miceli and J. H. Eberly, *Physical Review Letters,* 1987, **58**, 1499–1501.
3 A. J. Cox and D. C. Dibble, *Journal of the Optical Society of America A,* 1992, **9**, 282–286.
4 A. Vasara, J. Turunen and A. T. Friberg, *Journal of the Optical Society of America A,* 1989, **6**, 1748–1754.
5 R. M. Herman and T. A. Wiggins, *Journal of the Optical Society of America A,* 1991, **8**, 932–942.
6 X. Li, M. Pu, Z. Zhao, X. Ma, J. Jin, Y. Wang, P. Gao and X. Luo, *Scientific Reports*, 2016, **6**, 20524.
7 W. B. Williams and J. B. Pendry, *Journal of the Optical Society of America A*, 2005, **22**, 992–997.
8 T. Grosjean, D. Courjan and D. V. Labeke, *Journal Microscopy*, 2003, **210**, 319–323.
9 F. G. Mitri, *Optics Letters*, 2011, **36**, 766–768.
10 X. Luo, M. Pu, X. Li and X. Ma, *Light: Science & Applications*, 2017, **6**, e16276.
11 F. O Fahrbach, P. Simon and A. Rohrbach, *Nature Photonics*, 2010, **4**, 780–785.
12 Z. Bouchal, R. Horak and J. Wagner, *Journal of Modern Optics,* 1996, **43**, 1905–1920.
13 T. Cižmár, V. Kollárová, Z. Bouchal and P. Zemánek, *New Journal of Physics*, 2006, **8**, 43.
View Article Online
DOI: 10.1039/C6MH00535G
14 M. Q. Qi and W. X. Tang, *Scientific Reports*, 2015, **5**, 11732.
15 S. Ruschin and A. Leizer, *Journal of the Optical Society of America A*, 1998, **15**, 1139-1143.
16 T. Grosjean, D. Courjon and D. V. Labeke, *Journal of Microscopy*, 2003, **210**, 319-323.
17 M. F. Imani and A. Grbic, *IEEE Transactions on Antennas and Propagation*, 2012, **60**, 3155-3164.
18 G. Rui, Y. Lu, P. Wang, H. Ming and Q. Zhan, *Journal of Applied Physics*, 2010, **108**, 074304.
19 G. Rui, Y. Lu, P. Wang, H. Ming and Q. Zhan, *Optics Communications*, 2010, **283**, 2272-2276.
20 Q. Zhan, *Optics Letters*, 2006, **31**, 111726.
21 W. Chen and Q. Zhan, *Optics Letters*, 2009, **34**, 722-724.
22 I. Avrutsky, I. Salakhutdinov, J. Elser and V. Podolskiy, *Physical Review B*, 2007, **75**, 241402.
23 X. Luo and T. Ishihara, *Optics Express* 2004, **12**, 3055–3065.
24 G. F. Liang, C. T. Wang, Z. Y. Zhao, Y. Q. Wang, N. Yao, P. Gao, Y. F. Luo, G. H. Gao, Q. Zhao and X. G. Luo, *Advanced Optical Materials*, 2015, **3**, 1248-1256.
25 P. Gao, N. Yao, C. T. Wang, Z. Y. Zhao, Y. F. Luo, Y. Q. Wang, G. H. Gao, K. P. Liu, C. W. Zhao and X. G. Luo, *Applied Physics Letters*, 2015, **106**, 093110.
26 E. D. Palik, *Handbook of Optical Constants of Solids,* Academic Press, San Diego, 1998.
27 B. Wood and J. B. Pendry, *Physical Review B*, 2006, **74**, 115116.
28 X. Luo, *Science China-Physics, Mechanics & Astronomy*, 2015, **58**, 594201.
29 J. A. Dionne, L. A. Sweatlock and H. A. Atwater, *Physical Review B*, 2005, **72**, 075405.
30 R. Rivoire, A. Faraon and J. Vuckovic, A*pplied Physics Letters*, 2008, **93**, 063103.
31 I. Antonio, F. Domínguez, Z. W. Liu and J. B. Pendry, *ACS Photonics*, 2015, **2**, 341−348.
32 Z. Bouchal and M. Olivík, *Journal of Modern Optics*, 1995, **42**, 1555-1566.
33 Y. Xiong, Z. W. Liu and X. Zhang, *Applied Physics Letters*, 2008, **93**, 111116.
34 M. G. Moharam, E. B. Grann and D. A. Pommet, *Journal of the Optical Society of America A*, 1995, **12**, 1068-1076.
35 X. Y. He, Q. J. Wang and S. F. Yu, *IEEE J. Quantum Electron*, 2012, **48**, 1554.
36 A. J. Hoffman, L. Alekseyev, S. S. Howard, K. J. Franz, D. Wasserman, V. A. Podolskiy, E. E. Narimanov, D. L. Sivco and C. Gmachl, *Nature Materials,* 2007, **6**, 946-950.
37 X. Y. He, Z. Y. Zhao and W. Z. Shi, *Optics Letters*, 2015, **40**, 178-181.
38 M. Yan, L. Thylen and M. Qiu, *Optics Express,* 2011, **19**, 3818-3824.
39 X. Y. He, *Carbon,* 2015, 82, 229-237.
40 N. Yu, P. Genevet, M. A. Kats, F. Aieta, J.-P. Tetienne, F. Capasso, Z. Gaburro, *Science*, 2011, **334**, 333.
41 M. Pu, X. Li, X. Ma, Y. Wang, Z. Zhao, C. Wang, C. Hu, P. Gao, C. Huang, H. Ren, X. Li, F. Qin, M. Gu, M. Hong and X. Luo, *Science Advances*, 2015, **1**, e1500396.
42 Y.-W. Huang, W. T. Chen, W.-Y. Tsai, P. C. Wu, C.-M. Wang, G. Sun and D. P. Tsai, *Nano letters*, 2015, **15**, 3122.
43 J. Luo, B. Zeng, C. Wang, P. Gao, K. Liu, M. Pu, J. Jin, Z. Zhao, X. Li, H. Yu and X. Luo, *Nanoscale*, 2015, **7**, 18805.
44 X. Li, L. Chen, Y. Li, X. Zhang, M. Pu, Z. Zhao, X. Ma, Y. Wang, M. Hong and X. Luo, *Science Advances*, 2016, **2**, e1601102.

Published on 25 January 2017. Downloaded by Freie Universitaet Berlin on 26/01/2017 00:30:51.
Materials Horizons Accepted Manuscript

View Article Online
DOI: 10.1039/C6MH00535G

Published on 25 January 2017. Downloaded by Freie Universitaet Berlin on 26/01/2017 00:30:51.

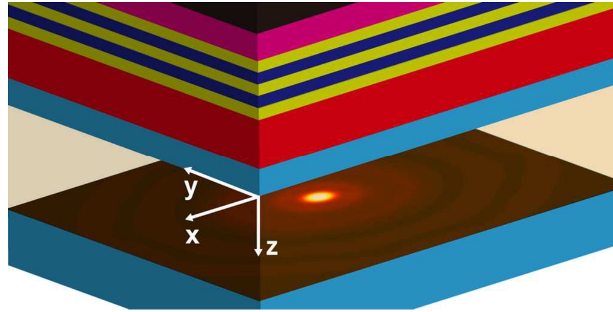

Evanescent Bessel beam with lateral dimension beyond the diffraction limit is generated by combining plasmonic metasurfaces and hyperbolic metamaterials.

Materials Horizons Accepted Manuscript